Combustion Synthesized Vanadia Rods for Environmental Applications

Parag A. Deshpande and Giridhar Madras
Dept. of Chemical Engineering, Indian Institute of Science, Bangalore, Karnataka 560012, India

DOI 10.1002/aic.12418
Published online October 19, 2010 in Wiley Online Library (wileyonlinelibrary.com).

Rod-shaped V_2O_5 was synthesized using the solution combustion technique, and the morphology *of the compound was confirmed by TEM. Rods of an average diameter of 500 nm and length 3–6 times the diameter were obtained after the calcination of freshly prepared V_2O_5 at 550°C for 24 h. Pd metal nanoparticles of 20 nm size were deposited onto the rods using the wet impregnation technique. The as-synthesized, calcined and Pd impregnated V_2O_5 were characterized by a wide variety of techniques including energy dispersive X-ray spectroscopy and X-ray photoelectron spectroscopy. These compounds were tested for CO oxidation, adsorption, and photocatalytic degradation of dyes. The 1% Pd/V_2O_5 showed a high activity for CO oxidation, the as-synthesized compound showed activity for the adsorption of cationic dyes, whereas the calcined V_2O_5 sample showed high rates of photocatalytic degradation of dyes.* © 2010 American Institute of Chemical Engineers *AIChE J,* 57: 2215–2228, 2011
Keywords: morphology, calcination, spectroscopy, CO oxidation, adsorption, degradation, mechanism

Introduction

The ability of vanadium to exhibit multiple oxidation states renders it suitable for various catalytic applications, especially those involving oxidation or redox reactions. In the oxides of vanadium, namely V_2O_3, VO_2, and V_2O_5, oxidation states of +3, +4, and +5 are exhibited by vanadium, apart from the feasible oxidation state of +2, which can be found in coordination compounds. Among the various oxides of vanadium, V_2O_5 has been studied widely in conjunction with the other oxides like Al_2O_3, TiO_2, ZrO_2, and MoO_3 for catalytic applications.[1–10] However, there have been relatively few studies reporting V_2O_5 supported systems.

Synthesis of V_2O_5 has been reported by several investigators using various techniques.[11–17] Different morphological features of V_2O_5 such as powder,[11] spheres,[12] plates,[13] and rods[14-16] have been reported. Several other interesting features like urchin surfaces, terraced surfaces, radial needles, and hollow structures have been obtained by suitably tuning the synthesis conditions, mainly the reaction temperature and reaction time.[12,15,17] The effect of morphology on the catalytic properties of compounds has been investigated by several investigators.[18–20] This becomes especially important in case of metal-support systems as the morphology governs the face plane exposure to the reactants, and hence, the reactivity of the catalyst.

V_2O_5-based catalysts have been widely used for NO_x abatement and selective catalytic reduction (SCR) along with other oxide materials.[1,2,10,21,22] Calatayud et al.[22] have explained the reaction involving NO and NH_3 over vanadium-based catalysts on the basis of the redox V^{5+} to V^{4+} cycles, and by the utilization of hydroxyl groups and hydrated surfaces. Most of the studies were carried out with mixed catalysts in which V_2O_5 was present along with a second component, mainly TiO_2 and Al_2O_3. The selectivity of the compound is very desirable for its applications in exhaust catalytic applications. The involvement of the second component is for the oxidation of CO and other hydrocarbons. The use of a single component catalyst with an ability to carry out both SCR and oxidation of CO eliminates

Additional Supporting Information may be found in the online version of this article.

Correspondence concerning this article should be addressed to G. Madras at giridhar@chemeng.iisc.ernet.in.

the necessity of the introduction of the other components. Therefore, CO oxidation reactions were carried out with Pd-impregnated V_2O_5. The use of Pt in exhaust catalysis is prevalent. The use of Pd is desirable because of the reduction in the cost of the catalyst. Pt is an established catalytic element in industrial application including exhaust catalysis.[23-25] The use of Pd provides an economic alternative and the associated processes, thus can be much more economic than the existing ones which make use of expensive Pt catalysts.

Although there have been several reports on the catalytic oxidation of organics over metal-V_2O_5 systems, only few studies[26,27] have been carried out testing the catalytic activity of V_2O_5 for CO oxidation. In this study, we discuss in detail the synthesis and characterization of V_2O_5 by solution combustion technique and the application of Pd-impregnated V_2O_5 for CO oxidation. We also propose a plausible mechanism on the basis of spectroscopic observations.

Adsorption and photocatalysis are used for the removal of hazardous chemicals from industrial effluents. Adsorption is used for the removal of the effluents from a stream having a high concentration of toxic chemicals. Photocatalysis becomes important when it is required to remove the final traces of the chemicals from the stream. V_2O_5 is a potential candidate as a photocatalyst. The photocatalytic activity of V_2O_5 has also been reported with its composites with TiO_2.[28-30] However, recently Fei et al.[12] have reported the photocatalytic activity of V_2O_5 hollow spheres. The compound showed a morphological dependence of the photocatalytic activity for the degradation of rhodamine B. V_2O_5 has also been used for the photooxidation of aniline.[31] Therefore, it is desirable to explore the photocatalytic activity of the compound. Photocatalytic degradation of anionic and cationic dyes was carried out over synthesized V_2O_5 and the compound was found to be photocatalytically active. although carrying out the degradation of dyes over as-synthesized V_2O_5, a large adsorption of the dyes was observed over the compound. This showed that as-synthesized catalyst can act as a good adsorbent of the dyes.

In this study, we have synthesized V_2O_5 rods and Pd-impregnated V_2O_5 and have shown the utility for three processes namely CO oxidation, adsorption of dyes, and photocatalytic degradation of dyes. All of these processes are used in chemical industries and development of new materials for these processes is of great interest to the chemical engineering community. The development of the materials reported in this study focused on the environmental applications. The same material with modifications is shown to be applicable for three processes of environmental applications namely CO oxidation and removal of dyes. Therefore, the objectives of the study are threefold. These involved (a) the synthesis of vanadia nanorods by a solution combustion technique and deposition of Pd metal nanoparticles, (b) characterization of the as-synthesized, calcined and Pd-impregnated nanorods, and (c) the use of these materials for three distinct environmental applications namely the oxidation of CO, adsorption of dyes, and photocatalytic degradation of dyes.

Experimental Section

Synthesis

Solution combustion technique was used for the synthesis of the compounds. Ammonium metavanadate (NH_4VO_3, S.D. Fine Chem, India) was used as vanadium precursor and glycine ($C_2H_5NO_2$, S.D. Fine Chem, India) was used as the fuel. A solution of the above two compounds was made in water. A few drops of nitric acid were added to the solution to increase the solubility of the compounds in water. The solution was kept in a preheated muffle furnace, maintained at a temperature of 350°C. The solution was observed to catch fire and a black mass of solid was obtained after combustion. This is referred to as the "as-synthesized" compound in the text. The powder was finely ground and heated at 550°C for 24 h in a muffle furnace. A brick red powder was obtained after calcination, referred to as the "calcined" compound in the text.

For the synthesis of Pd-impregnated compound, a known amount of calcined sample was taken as slurry. Palladium chloride ($PdCl_2$, S.D. Fine Chem, India) was added to the solution in an amount, which corresponded to Pd metal by weight, required in the final compound. The solution was stirred continuously and a dilute solution of hydrazine hydrate ($N_2H_4{\cdot}H_2O$, S.D. Fine Chem, India) was added slowly to the solution. The solution was observed to turn black. Catalysts with four different loadings of Pd metal, 1%, 2%, 5%, and 10% by weight, were prepared. The black solution was then sonicated in a water bath for 15 min to obtain a fine dispersion of the metal. The solids were then separated from the solution, filtered, washed repeatedly with ethanol, and heated in a muffle furnace at 550°C for 10 h to remove all the solvents and obtain the final product. The color of Pd-impregnated compound was also observed to be brick red.

Characterization

All the compounds were characterized by X-ray diffraction (XRD), X-ray photoelectron spectroscopy (XPS), transmission electron microscopy (TEM), energy dispersive X-ray spectroscopy (EDX), thermogravimetric analysis, and BET surface area analyzer. XRD patterns of the compounds were obtained from Philips X'pert diffractometer with CuKα radiations in a 2θ range of 20–80° with an interval of 0.03°. XPS of the elements present in the compounds were recorded on Thermo Fisher Scientific Multilab 2000 instrument utilizing AlKα radiation of energy 1486.6 eV. The TEM and EDX analysis of the compounds was carried out on Tecnai F-30 machine. Thermogravimetric analysis (TGA) of the samples was carried out using Perkin Elmer TG-DTA unit with a heating rate of 5°C/min. The surface areas of the compounds were determined using NOVA-1000 Quantachrome apparatus with N_2 adsorption–desorption cycles.

CO oxidation experiments

CO oxidation experiments were carried out in 9-mm ID glass tube reactors. The catalyst powder was plugged between ceramic wool. The temperature of the reactor was maintained using a PID controller with the thermocouple placed in the catalyst bed. A catalyst weight of 100 mg was used for all the reactions. A mixture of CO, O_2, and N_2 (all from Chemix Speciality Gases, Bangalore, India) was sent through flow controllers to the reactor. CO:O_2 ratio of 1:1 was maintained in all the experiments. All the reactions

were carried out at a constant flow rate of 110 mL/min. The products of the reaction were analyzed using an online gas chromatograph (Mayura Analytical, India). CO and CO_2 were separated using a molecular sieve column and were detected using a flame ionization detector. The spent catalyst was characterized after the reaction in XPS.

Adsorption experiments

Adsorption of anionic and cationic dyes was carried out over as-prepared compound. The anionic dyes used were orange G (OG), Remazol brilliant blue R (RBBR), and indigo carmine (IC). The cationic dyes chosen for the tests were acriflavin (AF), brilliant green (BG), and Rhodamine 6G (R6G). In all the experiments, a dye solution of a known initial concentration was taken in a beaker. A known amount of the as-prepared V_2O_5 was added to the solution. The solution was stirred continuously using a magnetic stirrer. Samples were taken out at regular intervals and centrifuged to remove the compound. The supernatant solution was analyzed using a UV–vis spectrophotometer (UV-1700, Shimadzu). The concentrations were determined using a relation between the concentration and absorbance of the dye solution obtained for the standard dye solutions. The effect of initial concentration and weight of adsorbent on the rates of adsorption were studied. For studying the effect of the initial concentration of the dye, an adsorbent concentration of 1 g/L was maintained. An initial dye concentration of 50 ppm was used for studying the effect of the weight of the adsorbent.

Photocatalytic degradation experiments

Photocatalytic degradation of dyes was studied over calcined V_2O_5 and the dyes chosen for the adsorption experiments were also used for the degradation experiments. A dye concentration of 50 ppm and a catalyst concentration of 1 g/L were maintained in all the experiments. The reactions were carried at natural pH of the dye solutions, which was found to be nearly 6.5. The reactions were carried out in a jacketed quartz tube flask with a provision for water circulation for cooling. A high-pressure mercury lamp was used as a source of UV radiations, which provided a flux of 40 W/m^2 at an intensity of 2 μE/L/s.

Results and Discussion

Structural analysis

X-Ray Diffraction. XRD patterns of all the compounds were recorded to obtain the crystal structure of the compounds. Figure 1a shows the XRD of as-prepared and calcined V_2O_5. In the calcined compound, the diffraction lines were indexed to the orthorhombic structure of V_2O_5 with a space group of P*mmn*. The XRD pattern showed the formation of highly crystalline phase. Therefore, the compound obtained after calcination was orthorhombic V_2O_5. However, the as-synthesized compound lacked crystallinity. By comparing the relative magnitudes of the intensities of XRD patterns of as-synthesized and calcined compound, it is clear that as-synthesized compound contained amorphous impurities. The diffraction lines in the XRD of as-prepared compound were indexed to those of orthorhombic V_2O_5 and ammonium metavanadate, which was used as the precursor. Therefore, during the combustion of the precursor solution, only a partial formation of V_2O_5 took place. The amorphous character was due to the formation of carbon from the fuel. This was confirmed by XPS, TEM, and EDX (discussed later). Calcination was an essential step for the formation of crystalline orthorhombic V_2O_5 rods. However, the formation of V_2O_5 during combustion is an important step as V_2O_5 crystallites formed during this stage act as nucleation centers for the growth of the crystals and impart the morphological characteristics to the final product.

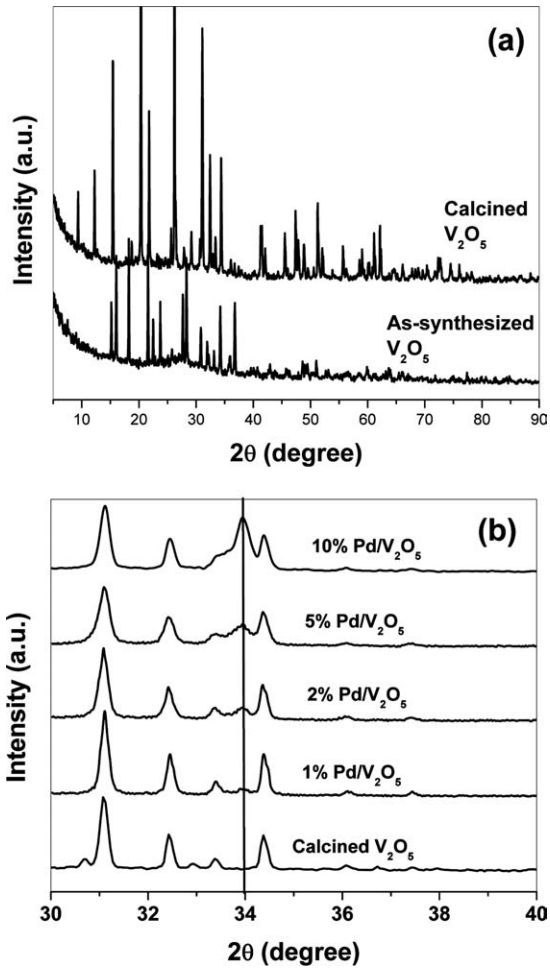

Figure 1. XRD of (a) as-synthesized and calcined V_2O_5 and (b) XRD of Pd-impregnated V_2O_5.

The vertical line in the figure shows the Pd metal peak.

The diffraction lines corresponding to Pd metal could be observed in the XRD of impregnated catalysts (Figure 1b). The intensity of the peak ($2\theta = 34°$) was observed to increase with Pd content. However, the crystal structure and the morphology (as confirmed by TEM) remained unchanged.

X-Ray Photoelectron Spectroscopy. XPS of all the elements in the compounds were recorded to determine the oxidation state and changes before and after CO oxidation. Vanadium exhibits variable oxidation states and XPS can be used to determine the oxidation state of V in the compound. However, the differences in the binding energies for the different oxidation states are small and it is important to adopt

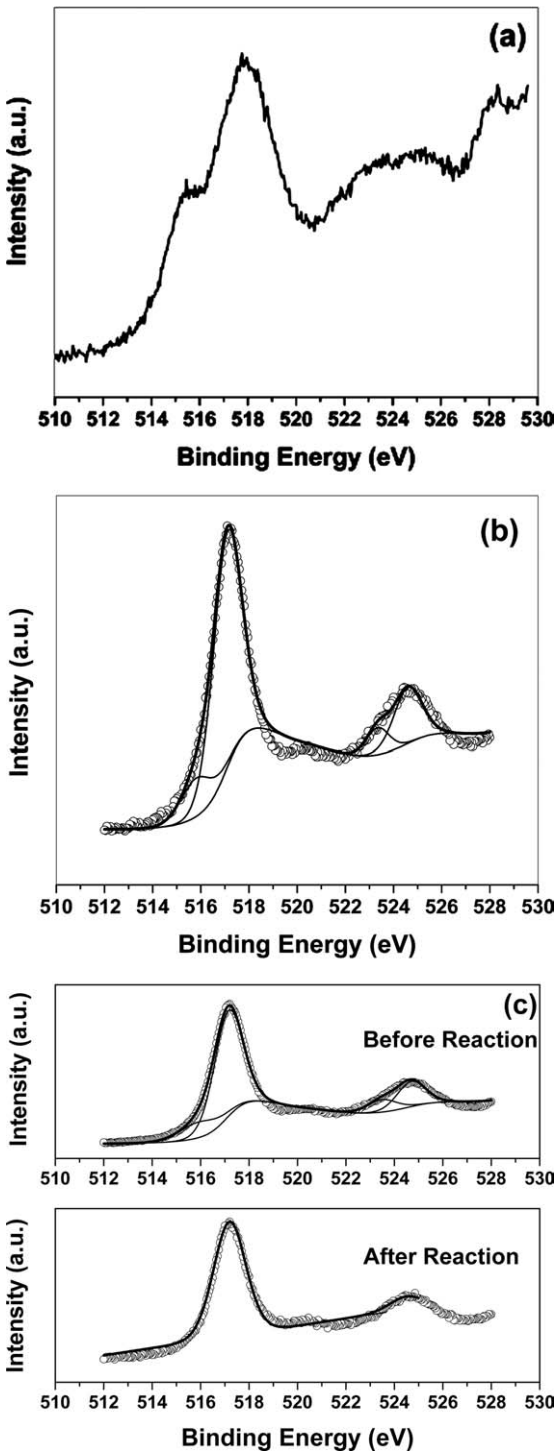

Figure 2. XPS of V2p in (a) as-synthesized V_2O_5, (b) calcined V_2O_5, and (c) 1% Pd/V_2O_5 before and after CO oxidation reaction.

a correct calibration standard for the binding energy. Generally, the binding energy of C1s at 284.5 eV is used as a standard. According to Silversmit et al.[32] for V2p spectra, C1s is not an appropriate choice. Instead the results can be described correctly if the binding energy of O1s is used. Therefore, all the spectra in this study were calibrated with respect to the O1s binding energy at 530 eV. Further, the compounds synthesized by solution combustion technique inherently contain small amounts of carbon. In the as-synthesized compound, we have observed a large amount of

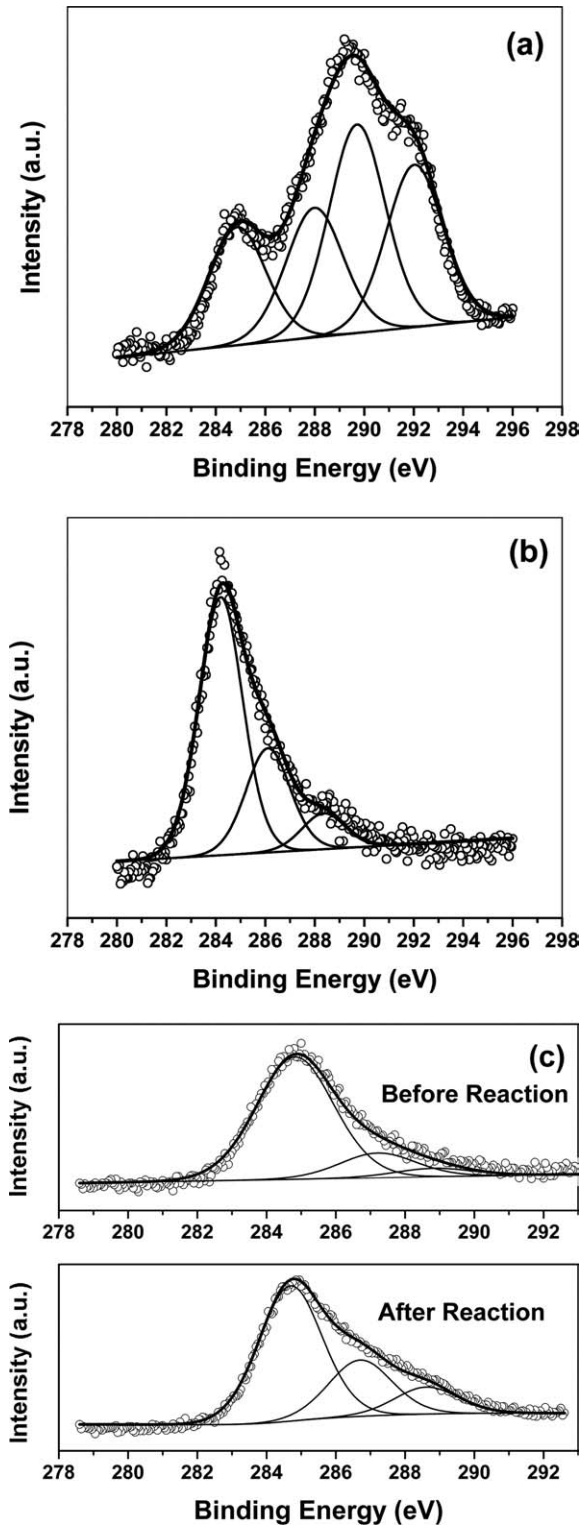

Figure 3. XPS of C1s in (a) as-synthesized V_2O_5, (b) calcined V_2O_5, and (c) 1% Pd/V_2O_5 before and after CO oxidation reaction.

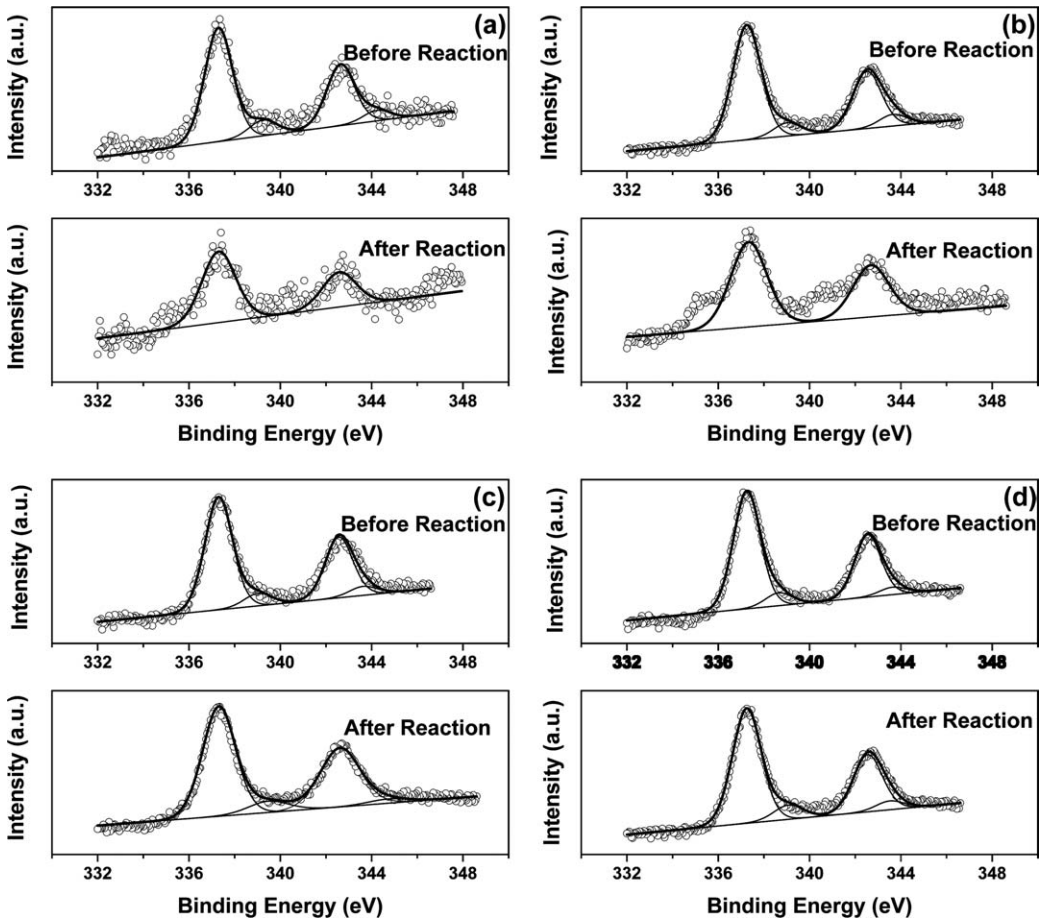

Figure 4. XPS of Pd3d in (a) 1% Pd/V_2O_5 before and after CO oxidation reaction, (b) 2% Pd/V_2O_5 before and after CO oxidation reaction, (c) 5% Pd/V_2O_5 before and after CO oxidation reaction, and (d) 10% Pd/V_2O_5 before and after CO oxidation reaction.

amorphous carbon and a very wide C1s spectrum was obtained. Therefore, O1s binding energy was used for the calibration.

The XPS of O1s in as-synthesized and calcined V_2O_5 is shown in Supporting Information Figure S1. The main peak was observed at 530 eV. A small peak at 532 eV was observed in the spectrum of calcined V_2O_5, corresponding to oxygen in C—O(H) form.[32] This peak was also observed in all Pd-substituted compounds, before and after CO oxidation reaction. The implications of the changes in the signals before and after the reaction are discussed later. A small peak at 525 eV was observed in the spectrum of as-synthesized V_2O_5. This value of binding energy cannot be attributed to carbon in any form and may have arisen due to impurities.

Vanadium in all the compounds was present in +5 state, confirming the formation of V_2O_5. Peaks of very small intensities were observed at 516 eV, corresponding to vanadium in +4 state[32] (Figures 2a–c) and Supporting Information Figures S2a–c. However, this amount was negligible and after CO oxidation, only +5 state was observed.

In the XPS of C1s in the as-synthesized compound, several peaks were observed corresponding to carbon in various forms. Three clearly distinguishable peaks at 284.5 eV, 286.5 eV, and 288 eV correspond to graphitic carbon, C=O and C—O(H), respectively.[33,34] It is clear from Figure 3a that as-prepared compound contained a large amount of carbon in different forms as a result of combustion. The amount of carbon in the calcined compound reduced, as can be seen from a decrease in the intensity of the peak (Figure 3b). Moreover, most of the carbon was present as graphitic carbon. In Pd-substituted compounds, other forms of carbon were also observed (Figure 3c and Supporting Information Figures S3a–c). This form of carbon corresponded to that associated with C=O and C—O(H) form and is in agreement with those observed in O1s spectra.

The XPS of Pd3d is shown in Figures 4a–d. A wide spectrum was obtained in all the compounds corresponding to $Pd3d_{5/2\text{-}3/2}$. The spectra were decomposed to get the individual oxidation states of Pd. In all the freshly prepared samples, small non-zero intensities were indeed observed at 339 and 344 eV corresponding to ionic Pd.[35] The decomposed spectra at these values of binding energies suggest Pd in +2 state. This can be either due to the presence of the precursor $PdCl_2$ in which the oxidation state of Pd is +2 or due to the ionic substitution of Pd in the lattice due the thermal treatment step. The inclusion of metal in ionic state in the matrix due to thermal treatment has been reported by Pierre et al.[36]

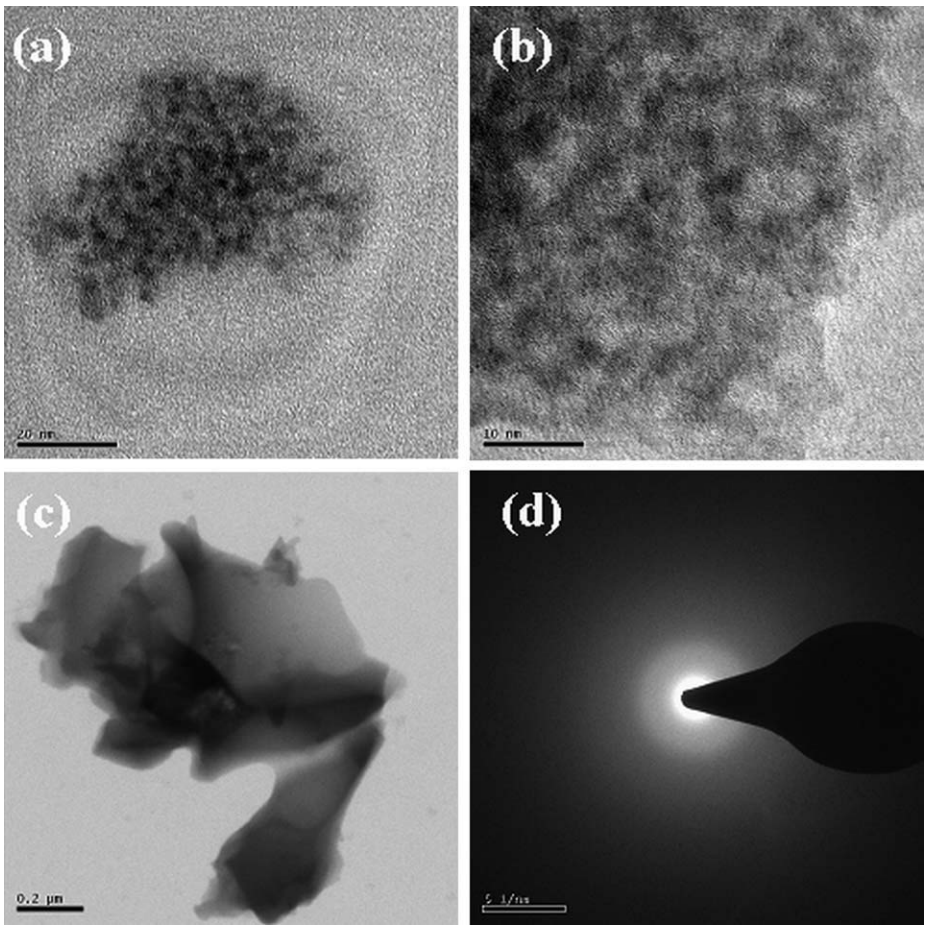

Figure 5. TEM images and the electron diffraction pattern of as-synthesized V_2O_5.

(a–c) TEM images and (d) electron diffraction pattern.

However, the ionic Pd intensity was observed to be negligible after CO oxidation reaction, and Pd was found to be in metallic state. Consistent trends were observed in the spectra for all the compounds. This was used for developing CO oxidation mechanism discussed later.

Transmission Electron Microscopy. TEM images of as-synthesized compound are shown in Figure 5. Large agglomerates of microscopic sizes were observed, as can be seen from Figure 5c. These agglomerates did not exhibit any morphological features. Further, the electron diffraction pattern taken on the agglomerates showed lack of crystallinity. This is clear from Figure 5d where no diffraction lines could be observed. Therefore, from the TEM analysis of the as-prepared samples, it is clear that the compound was not fully crystallized and the morphological features were not developed. This is in accordance with the XRD pattern obtained for the as-synthesized compound (Figure 1a). However, very small amorphous particles can be seen in the TEM images shown in Figures 5a, b. These can be due to the formation of amorphous carbon during the combustion synthesis. C1s peaks of different intensities were observed in the XPS at different binding energies (Figure 3a). The small particles seen in the TEM image could be the particles of amorphous carbon.

Figures 6a–c show the TEM images of the calcined sample. It is clear from the images that V_2O_5 attained the morphology of rods. The rods had an average diameter of 500 nm. Although, rods of different lengths can be observed, most of the rods had lengths in the range of 3–5 μm. The rods were observed to be distinct and bulk fusion of the particles did not take place. The electron diffraction pattern taken on the rods showed the crystallinity. The electron diffraction pattern is shown in Figure 6d. A spot pattern was observed showing the crystallization of the compound on heat treatment. Spot patterns for orthorhombic V_2O_5 nanowires have been observed by Zhau et al.[37] Bulk amorphous carbon was not observed in the calcined samples in our studies.

Samples containing Pd metal were also analyzed for morphology, Pd particle size and agglomeration of Pd particles using TEM. It can be seen from Figures 7a–c that the rod shaped morphology of Pd-impregnated compound was maintained. Pd particles can be observed to be adhered on the surface of the rods. It can be observed that the Pd particles were far apart and were not in an agglomerated state showing a fine dispersion of Pd particles. In this case also, the rods were found to be distinct such that both rods and Pd particles were not in a fused form. Pd particles of size as

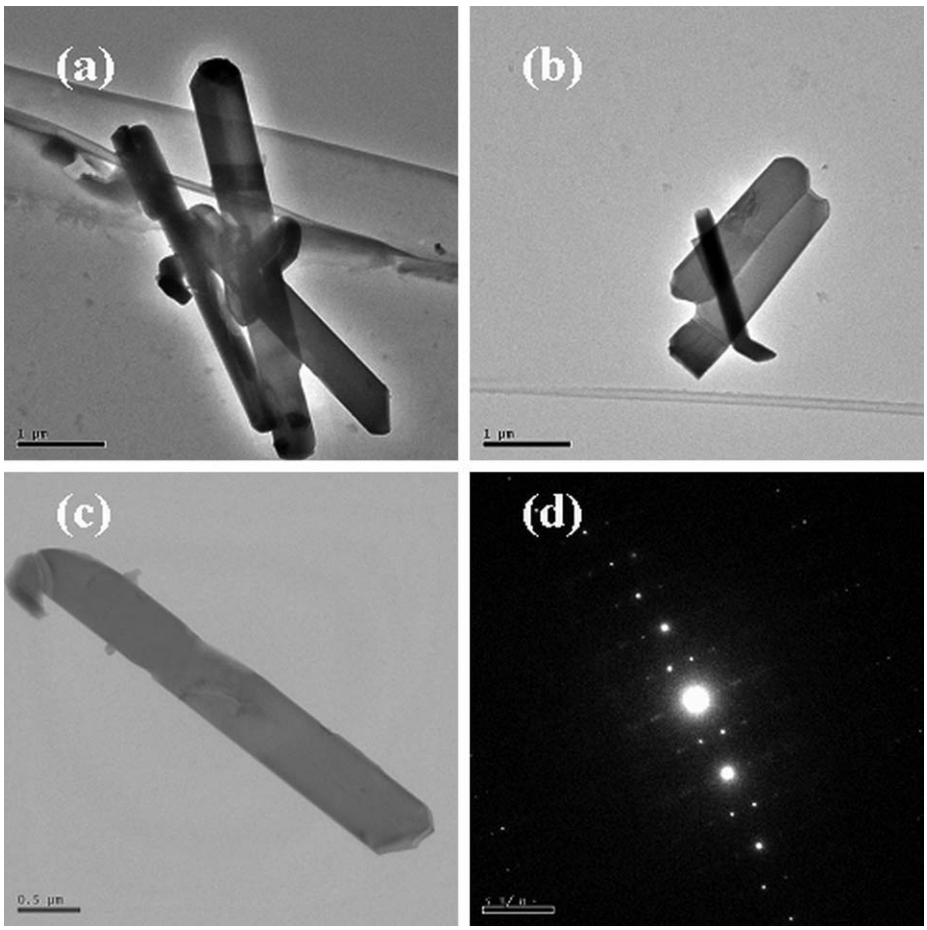

Figure 6. TEM images and the electron diffraction pattern of calcined V_2O_5.

(a–c) TEM images and (d) electron diffraction pattern.

small as 20 nm were observed and crystallinity in the sample was observed, as can be seen from the electron diffraction pattern shown in Figure 7d.

Energy Dispersive X-Ray Spectroscopy. EDX spectra of the samples were recorded to determine the quantitative elemental composition of the samples. All the spectra (see Supporting Information Figure S4) showed the presence of vanadium, oxygen, and carbon in the samples and Pd in Pd-impregnated sample. All the peaks corresponding to these elements are marked in the spectra. Small peaks corresponding to Cu can also be observed due to Cu from the grid used for mounting the samples. Cu was not taken into account for quantification of the sample. All the elements in the sample were found to be in the amounts corresponding to the stoichiometric amounts except that in the as-synthesized V_2O_5 where large amount of carbon was observed. The amount of Pd introduced in the impregnated compound was found to be in agreement with the amount of Pd added during the synthesis. It can be seen from the spectra of all the compounds that carbon was present in all the compounds. This is a characteristic of all the combustion synthesized compounds. However, a highly intense carbon peak can be observed in the spectra of as-synthesized V_2O_5. This is a confirmation of the observation of amorphous carbon from XRD, XPS, and TEM. We further prove it using TGA.

Thermogravimetric Analysis. TGA of the synthesized compounds is shown in Supporting Information Figure S5. A large weight loss was observed in the as-prepared sample on heating. The weight of the sample decreased to 43% of its original weight on heating it up to 600°C. However, such a large decrease was not observed in case of calcined samples. The weight loss was limited to 3–6% only. This clearly shows that the weight loss in the as-synthesized compound is not due to the dissociation of the compound or loss of molecular oxygen. The analysis was carried out in N_2 atmosphere. Therefore, it was not possible to have an oxidation of lower oxidation state vanadium oxides to V_2O_5 and correspondingly no gain in weight of the samples due to oxidation was observed in any of the cases. The only possible reason for a large decrease in the weight is the loss of amorphous carbon, which was present in the as-synthesized sample and was detected using the various characterization techniques.

BET Surface Area Analysis. The surface area of as-synthesized V_2O_5 was 10 m^2/g. A small decrease in the surface areas of the compounds was observed on calcination and all the calcined samples had surface areas in the range of 4–7 m^2/g.

CO oxidation over Pd-impregnated V_2O_5

CO oxidation was carried out over Pd-impregnated V_2O_5. Figure 8 shows the variation of CO concentration with

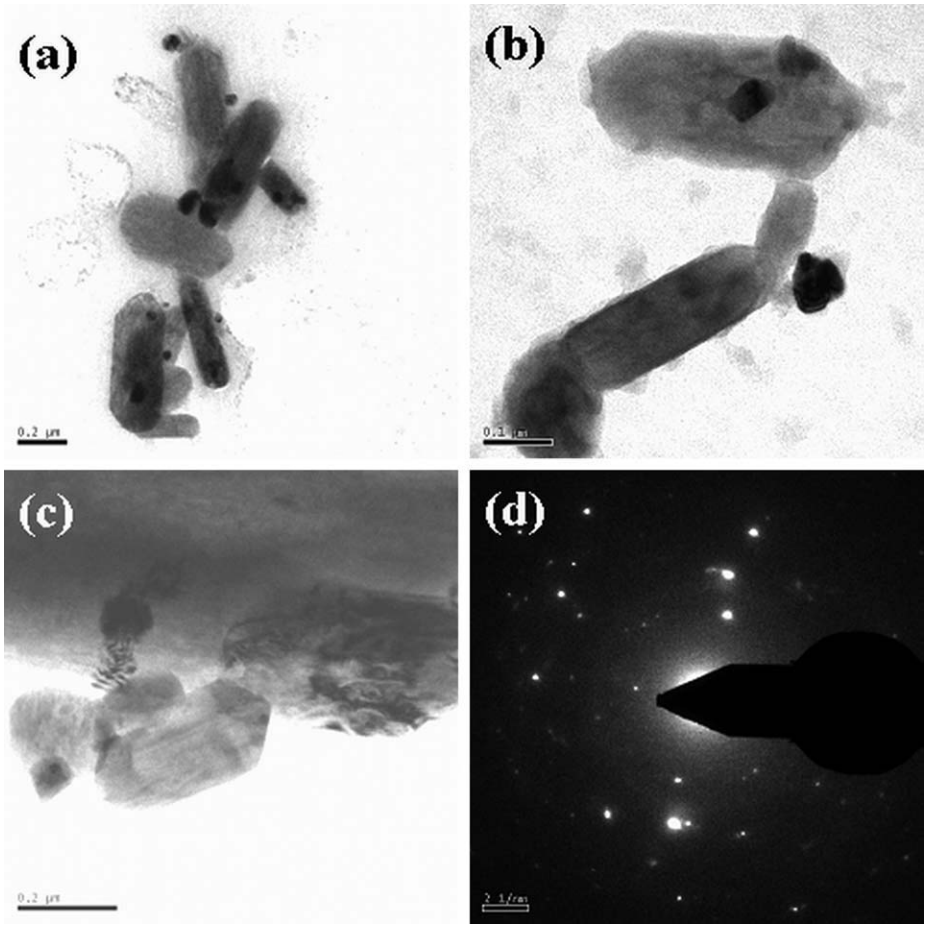

Figure 7. TEM images and the electron diffraction pattern of 10% Pd/V_2O_5.

(a–c) TEM images and (d) electron diffraction pattern.

temperature over 1% Pd/V_2O_5. The catalyst showed high activity for the reaction and complete conversion was possible within 300°C and 350°C when the concentration of CO in the feed was lesser than 5% and 10% by volume, respectively. At temperatures lesser than 225°C, a very small increase in conversion was observed with an increase in temperature. The conversions were limited to 15% within this temperature range. However, a sharp light off was observed for all the concentrations after 225°C. Nearly 50% conversion was observed within 260°C, and 80% conversion within 280°C. Nearly the same activity for different inlet concentrations of CO shows the presence of a large number of active Pd sites. With an increase in the concentration of CO, the sites remain available to maintain a high-reaction rate. A high dispersion of Pd over the support and the morphology of the support aiding the exposure of active phase planes can be attributed to the high activity of the catalysts. The Pd loading was increased to 10%; however, the temperature for complete conversion did not decrease significantly. This indicates that even at 1% Pd loading, a large number of active sites are available for the adsorption of CO and, therefore, the results of only 1% Pd/V_2O_5 are presented. In spite of low-surface area of V_2O_5, the activity of catalyst was found to be high. The exposure of the face planes due to the morphology of the support and the presence of Pd nanoparticles are the possible reasons for the high activity of even low-surface area compound. The presence of rod-like morphology in the system leads to the exposure of faces which

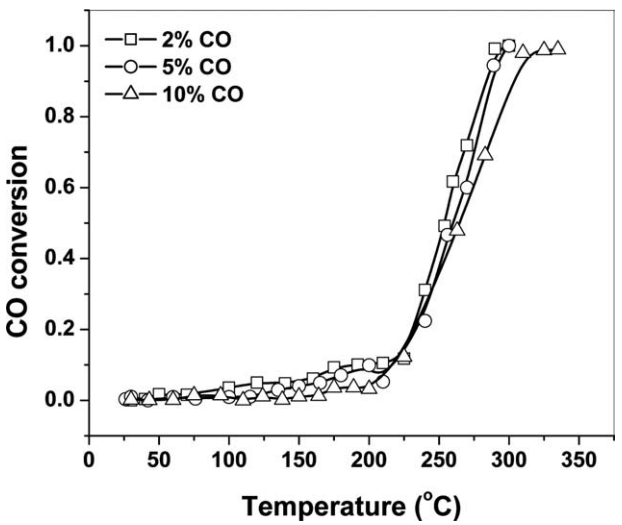

Figure 8. Variation of CO conversion with temperature over 1% Pd/V_2O_5.

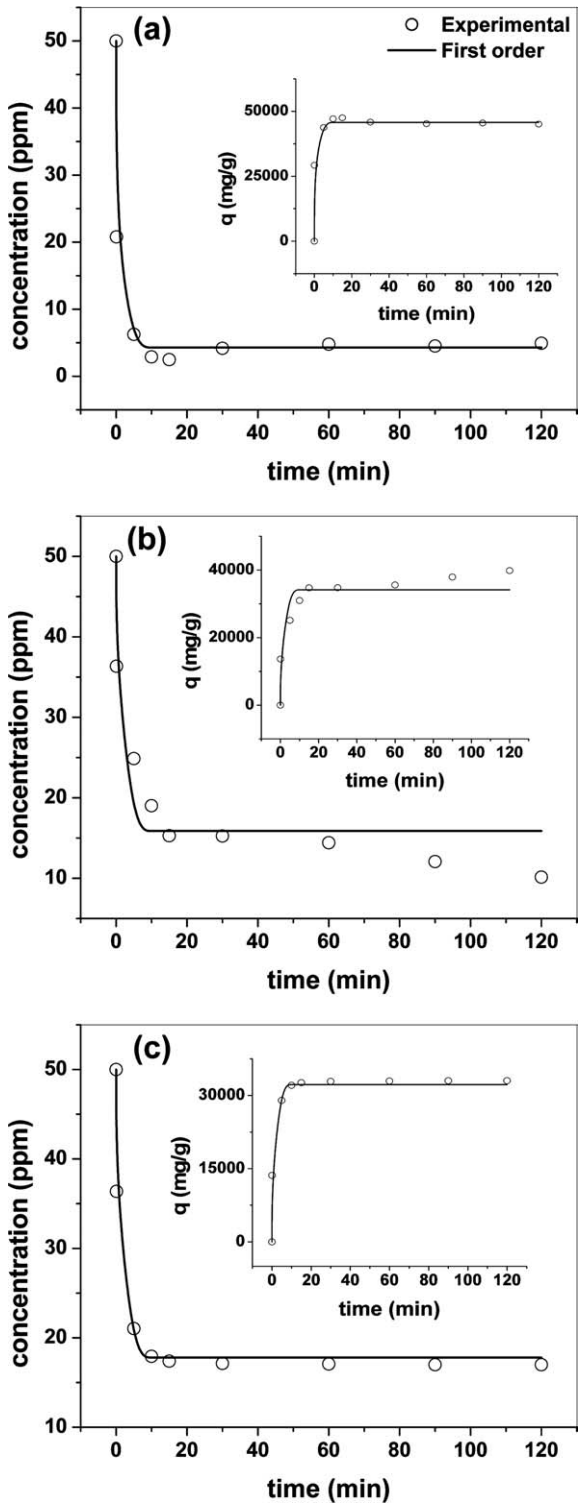

Figure 9. Variation of the concentration of various dyes with time during adsorption over as-synthesized V_2O_5 (a) AF, (b) BG, and (c) R6G.

The inset shows the variation of "q" with time.

can be labile to oxygen exchange, and hence, a high activity of the catalyst can be obtained.

No significant conversions were obtained over V_2O_5. Several investigators have studied the temperature programmed desorption of O_2 on V_2O_5.[38-41] According to Lewis et al.,[41] V_2O_5 surfaces are relatively inert and surface reconstructions are required for lattice oxygen exchange. The lattice oxygen exchange is very slow with O_2. In the presence of reducing agents like CO and H_2, the oxygen exchange is fast and the oxygen from the lattice can be used for the oxidation of CO to CO_2. However, because the adsorption of both CO and O_2 is poor over V_2O_5, the activity of the compound is very poor. Further, the vacancy formation energy for V_2O_5 has been calculated by first principles density functional theory calculations. The results show that the removal of oxygen by itself is difficult due to large vacancy formation energy.[42] A range of vacancy formation energies are present for V_2O_5 depending upon the position of different oxygen atoms.[42,43] The removal of oxygen in general is difficult, but is facilitated by the presence of other groups like hydroxyl groups. This also results in the reduction of the nearby vanadium atoms. Taufiq-Yap and Waugh[40] have reported the mechanism of CO oxidation over V_2O_5. The mechanism mainly consisted of oxidation of CO to CO_2 by lattice oxygen usage and a corresponding reduction of V^{5+} to V^{4+} creating an anion vacancy. The vacancies are filled by the dissociation of O_2 from the stream. Uptake of a reducing reactant from the stream forming anion vacancies and reduction to V^{4+} has also been observed by Xiao et al.[44] for SO_2 removal over V_2O_5.

When Pd is impregnated in the compound, the adsorption of CO is greatly enhanced. Adsorption of CO takes place over Pd. Surface reconstruction of oxides on adsorption of gases is known.[45] As a result, the CO oxidation ability of the compound is enhanced and high rates of CO oxidation are observed over Pd-impregnated compound. The effect is a result of enhanced adsorption and surface reconstruction.

Bronsted acid and Lewis acid sites in V_2O_5 are known to play an important role in SCR reactions.[46] In the presence of reagents like NH_3, such sites are very active and surface hydroxyl groups also take part in the reaction. However, for CO oxidation over calcined-V_2O_5 samples, the contribution for such groups is very unlikely. From the XPS of O1s before and after the reaction (Figure 2), the signals corresponding to C=O groups can be observed to increase. This shows the involvement of the oxygen from the lattice resulting from the adsorption of CO and exchange of oxygen. However, V^{4+}, which was observed in traces in the calcined-V_2O_5 before the reaction, got oxidized to V^{5+} and Pd^{2+} was found to reduce to Pd^0. Therefore, at the initial stages, reduction of Pd^{2+} to Pd metal takes place. This occurs at low temperatures and reduction of V^{5+} to V^{4+} does not take place. During this stage, the lattice oxygen exchange is lesser due to minimal reduction of V. With an increase in temperature, Pd^{2+} completely reduces to Pd^0. A reduction of V takes place this point onward. The CO oxidation profile in Figure 8 can be divided into two regions: one with lesser CO conversion (temperatures up to 225°C) and the high-temperature region (temperatures above light off). The enhancement in the rate from one region to the other is very large. Therefore, it can be said that a change in the mechanism takes place on transition. Initially, the lattice oxygen usage is minimal. At higher temperatures, lattice oxygen exchange takes place. This also results in the formation of anion vacancies. The formation of defects in the lattice

Table 1. Adsorption Parameters for the Adsorption of Different Cationic Dyes over As-Prepared V_2O_5

Dye	q_e (mg/g)	C_e (ppm)	k_n ($g^{n-1}/mg^{n-1}/min$)	n
AF	45,750 ± 334	4.25 ± 0.33	14.51 ± 0.21	1.70 ± 0.002
BG	34,290 ± 2	15.71 ± 0.002	15.39 ± 0.001	1.69 ± 0.001
R6G	32,310 ± 870	17.69 ± 0.87	15.74 ± 0.88	1.70 ± 0.01

results in an enhanced adsorption of O_2. As a result, the dissociation of O_2 on the vacancies takes place and a large increase in the rate of CO oxidation is observed. To summarize, the oxidation of CO over V_2O_5 takes place in two regimes with high rates of reaction possible when the lattice oxygen utilization takes place.

Adsorption of dyes over as-synthesized V_2O_5

The adsorption of anionic and cationic dyes was carried out over as-prepared V_2O_5. The adsorption of the dyes was found to be dependent upon the ionic nature of the dye. The adsorption of anionic dyes, OG, ACG, and RBBR, were tested over as-synthesized V_2O_5. No adsorption of the anionic dyes was observed over the adsorbent. However, when the adsorbent was tested for the adsorption of cationic dyes (AF, BG, and R6G), a large decrease in the concentration of the dyes was observed within a very short interval of time (Figures 9a–c). For all the three cationic dyes, equilibrium adsorption was achieved within 10 min of stirring. No significant change in the concentration of the dyes was observed after 15 min indicating the attainment of equilibrium.

Adsorption was observed only in case of as-synthesized V_2O_5. Adsorption over calcined V_2O_5 was minimal. All the characterization techniques showed the presence of a large amount of carbon in the as-synthesized compound. TEM analysis showed that carbon particles were finely dispersed with nanometer dimensions. Nearly 60% of the compound was found to consist of a very fine dispersion of carbon in the compound. Carbon formation was a result of combustion of the fuel during the synthesis of the compound and a release of a large amount of gases and quenching resulted in fine dispersion. Therefore, it is the presence of this carbon which is responsible for the adsorption of dyes. V_2O_5-activated coke systems have been studied by Yong et al.[47] It was possible to disperse V_2O_5 in the porous structure of activated coke. On similar grounds, it can be expected that during combustion, coke formation took place along with the formation of V_2O_5 resulting in the adsorption activity.

C1s in the as-prepared V_2O_5 showed the presence of several forms and the associated groups. Graphitic carbon, C═O and C─O(H) were observed in the compound. Surface hydroxyl groups were also observed in the XPS of O1s. Whereas the adsorption activity of graphitic carbon is well established, the presence of surface groups can also aid the adsorption process. High selectivity of the compound for cationic dyes was observed. This shows the involvement of the various charges present in the system in the adsorption process. Because of high electronegativity of oxygen, a partial negative charge is developed in the groups. As a result, the positive groups in the dyes are attracted toward the adsorbent resulting in the adsorption of the dye.

The variation of q, defined as the amount of adsorbate adsorbed per unit mass of the adsorbent, with time is shown in the insets in Figure 9. A sharp increase in the value of q can be observed, followed by a nearly constant value, corresponding to the equilibrium value, q_e.

The kinetics of adsorption can be studied either by following the variation of the dye concentration $C_A(t)$, or $q(t)$ with time. There are several reports on the adsorption of dyes, organic and metal ions on solids and kinetic models have been reported describing the variation of $C_A(t)$ and $q(t)$ with time.[45,46] The variation of $C_A(t)$ and $q(t)$ with time for nth order kinetics is given as

$$\frac{dC_A(t)}{dt} = k_n\{C_A(t) - C_{A_{eq}}\}^n \quad (1)$$

$$\frac{dq(t)}{dt} = k_n'\{q_e - q(t)\}^n \quad (2)$$

From Eqs. 1 and 2 the relation between the dye concentration $C_A(t)$ or $q(t)$ and time t can be found as

$$C_A(t) = C_{A_e} + \{(C_{A_0} - C_{A_e})^{1-n} + (n-1)k_n t\}^{1/1-n} \quad (3)$$

$$q = q_e - \{q_e^{1-n} + (n-1)k_n t\}^{1/1-n} \quad (4)$$

The experimental data obtained from the batch adsorption experiments along with Eqs. 3 and 4 were used to determine the parameters appearing in Eqs. 3 and 4 using a nonlinear regression technique based upon Levenberg-Marquardt technique. Table 1 shows the results obtained by regression. It can be seen that the equilibrium adsorption of the different dyes predicted by the model were close to those the equilibrium adsorption obtained experimentally. The order of adsorption was AF > BG > R6G.

According to Leyva-Ramos et al.,[48] kinetic models provide advantages of simplicity and ease of use. However, the physical interpretation of the phenomena is not possible. For this, diffusional models must be sought, which assume the kinetics to be diffusion limited. For intraparticle diffusion, the relation between q and diffusion time is given by

$$q(t) = k_D t^{1/2} \quad (5)$$

where k_D can be approximated using the following relation,[49]

$$q(t) = 6\left(\frac{D_1}{\pi a^2}\right)^{1/2} t^{1/2} \quad (6)$$

$$\ln\left(1 - \frac{q(t)}{q_{eq}}\right) = \ln\frac{6}{\pi^2} - \left(\frac{D_2\pi^2}{a^2}\right)t. \quad (7)$$

Equations 6 and 7 hold for small and large time intervals, respectively. D_1 and D_2 are the coefficients for film diffusion and pore diffusion, respectively. Therefore, D_1 can be obtained from the initial slope of the Figure 10a, and D_2 can be obtained from the slope of Figure 10b. The initial linear portion in Figure 10a shows that adsorption is limited by external film diffusion. The later flat portion shows the presence of intraparticle diffusion. We compare the relative magnitudes of D_1 and D_2 at initial stages of the process to have an idea about the mass transfer limitations. If α_1 and α_2 be the slopes of the curves defined by Eqs. 6 and 7 then

$$\alpha_1 = 6\left(\frac{D_1}{\pi a^2}\right)^{1/2} \tag{8}$$

$$\alpha_2 = \left(\frac{D_2\pi^2}{a^2}\right) \tag{9}$$

From Eqs. 8 and 9,

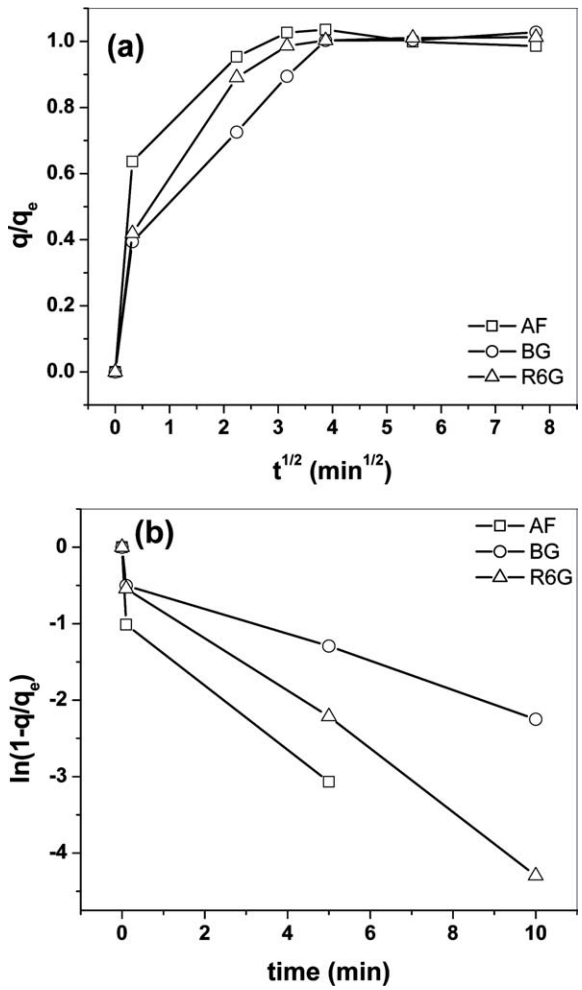

Figure 10. Dependence of q on t following intraparticle diffusion model.

(a) Film diffusion regime and (b) intraparticle diffusion regime.

Table 2. Relative Magnitudes of Film and Intraparticle Diffusion Coefficients for the Adsorption of Different Dyes over As-Prepared V_2O_5

	AF	BG	R6G
α_1	2.01	1.25	1.32
$\alpha_2(0)$	10.12	5.01	5.43
$\alpha_2(t)$	0.42	0.16	0.34
$D_1/D_2(0)$	0.34	0.27	0.28
$D_1/D_2(t)$	8.31	8.27	4.42

$$\frac{D_1}{D_2} = \frac{\pi^3\alpha_1^2}{36\alpha_2} \tag{10}$$

Two distinct slopes can be observed in Figure 10b. Thus, two regions, $t = 0$ and $t > 0$, can be defined and we carry out the analysis for these two regions. Table 2 gives the relative magnitudes of the film and intraparticle diffusion coefficients in the two regimes. At time $t = 0$, $D_1 < D_2$. This shows that adsorption is limited by diffusion in the film. At times $t > 0$, $D_1 > D_2$, showing that the intraparticle mass transfer resistances are high. The time interval for the first case is extremely small showing that the rate is extremely fast and the adsorption at the surface of the adsorbent takes place almost instantaneously. This is followed by a slower step of diffusion of the dye in the bulk of adsorbent and no appreciable adsorption takes place further.

Apart from the kinetic and intraparticle diffusion models described above, models like Elovich model were also tested for describing the adsorption. However, the regression parameters obtained for such models were inferior and thus, such models were not investigated further.

The effect of adsorbent weight on the initial rate of adsorption is shown in Figure 11. An increase in the initial rate was observed till 0.5 g/L adsorbent concentration. On increasing the adsorbent concentration further, no appreciable increase in the activity of the adsorbent was observed.

We now analyze the adsorption of the dyes over as-synthesized V_2O_5 in relation with the structure of the dye, the charge of the dye in the solution and the various groups

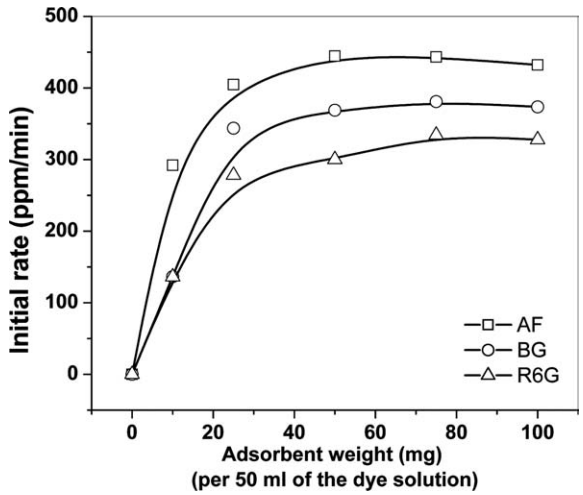

Figure 11. Variation of the initial rate of adsorption of cationic dyes with adsorbent weight.

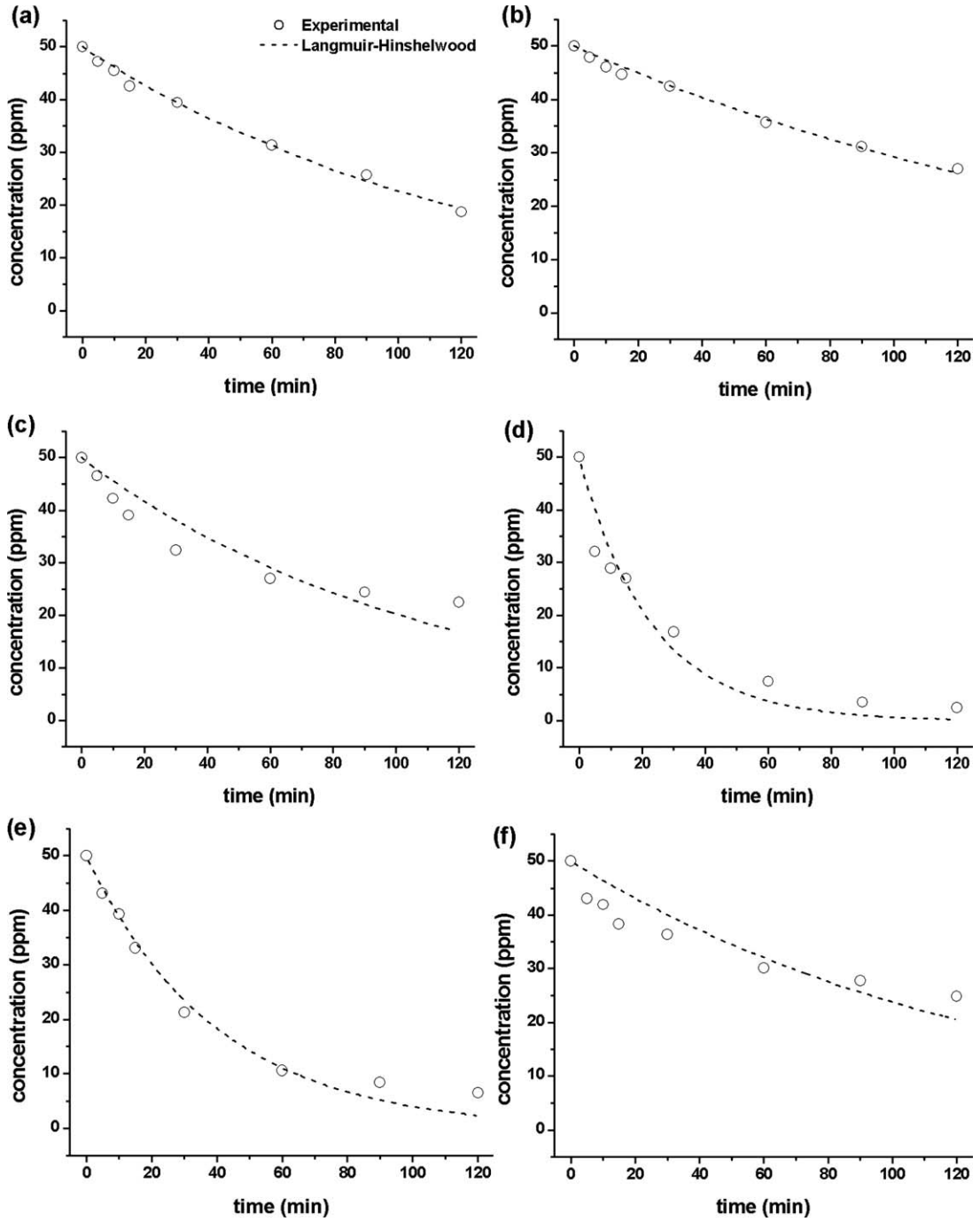

Figure 12. Variation of dye concentration with time over calcined-V_2O_5.

(a) OG, (b) IC, (c) RBBR, (d) AF, (e) BG, and (f) R6G.

present on the surface of the adsorbent. To confirm that the dye was indeed adsorbed on the surface of the adsorbent, the UV–vis spectra of the adsorbent after the adsorption was recorded. A peak at 525 nm corresponding to R6G was observed in the UV–vis spectra after the reaction (Supporting Information Figure S6). This confirmed the adsorption of the dye over the adsorbent.

The equilibrium adsorption of the dyes over the adsorbate and the rates of adsorption was found to be different for the different dyes. To explore the reason behind this, we study the structure of the dye. It can be seen in Supporting Information Figure S7 that for all the dyes, the potential centre for adsorption is the nitrogen atom with a unit positive charge. AF and R6G have anthraquinone rings with heteroatoms, BG has a triarylmethane composition. Therefore, steric hindrance can play a major role in the adsorption ability of the dye over the compound. In case of BG and R6G, nitrogen is surrounded by bulky ethyl groups but only a methyl group is present in the case of AF. Thus, the spatial occupation of the groups in case of BG and R6G is large compared

with that for AF. As a result, an easy access of the groups is possible for AF and the available number of sites is also used for adsorption resulting in higher adsorption.

Photocatalytic degradation of dyes over calcined-V_2O_5

Calcined-V_2O_5 was used for the photocatalytic degradation of anionic and cationic dyes. Figure 12 shows the variation of the concentration of various dyes with time. Cationic dyes showed high degradation with nearly 95% degradation of AF and BG within 2 h. Nearly 60% degradation of R6G was observed. The degradation of anionic dyes was relatively lesser compared with the degradation of the cationic dyes. Only 50–55% degradation of IC and RBBR was observed within 2 h. 65% degradation of OG took place over the catalyst.

Degradation of the dyes takes place via a series of reactions and different pathways are followed during the degradation of the dye depending upon the structure of the dye. We have previously found the dependence of degradation of the dyes on the functional groups present in the dye.[50] Langmuir-Hinshelwood model is commonly used for describing the degradation of the dye. The Langmuir-Hinshelwood model can be written as

$$r = \frac{Kk_1C_A}{1 + KC_A}. \tag{11}$$

The rate parameters for the degradation of the dyes over calcined-V_2O_5 following Langmuir-Hinshelwood model are given in Table 3. It can be seen from the relative magnitudes of the rate constants that the rate of degradation of cationic dyes is 5–7 times higher than the rate of degradation of anionic dyes except for the degradation of R6G. From the relative magnitudes of the values of K for the different dyes, it can be seen that the adsorption of OG, IC, and R6G was an order of magnitude higher that that of AF, BG, and RBBR. The rates of degradation of the dyes were observed to be in an opposite order. This clearly shows the effect of adsorption on the kinetics of the reaction. Adsorption of the dye over the surface of the catalyst is an essential step and the reaction takes place only at the surface of the catalyst where the dye is in contact with the catalyst. However, at higher surface coverage, the blocking of the active catalyst sites may take place and the phenomenon in that regime is only the photolysis of the dye, which is slower compared with the photocatalytic degradation. The degradation of the cationic dyes was also tested over the commercial Degussa P-25 TiO_2 catalyst. The rates of reaction over V_2O_5 were lesser for AF, comparable for BG and higher for R6G (Supporting Information Figure S8 and Table 4).

Table 3. Rate Parameters for the Photocatalytic Degradation of Anionic and Cationic Dyes over Calcined-V_2O_5

	Langmuir-Hinshelwood	
	k_1 (min^{-1})	K ($\times 10^5$) (ppm^{-1})
OG	275	2.87
IC	300	1.79
RBBR	1772	0.51
AF	13,791	0.31
BG	11,049	0.23
R6G	597	1.25

Table 4. Rate Parameters for the Photocatalytic Degradation of Cationic Dyes over Commercial Degussa P-25 Catalyst

	Langmuir-Hinshelwood	
	k_1 (min^{-1})	K ($\times 10^5$) (ppm^{-1})
AF	36,239	0.17
BG	15,714	0.26
R6G	298	1.53

We have shown the application of a single compound, V_2O_5, for three different applications. The fresh compound, due to high-carbon content is an excellent adsorbent. The same material after calcination loses carbon and acts as a photocatalyst for the degradation of various dyes. With the addition of a very small amount (1 wt %) of Pd nanoparticles, the same material was found to show catalytic properties for CO oxidation. Thus, it is possible to synthesize similar materials and the tune the properties for a particular application.

Conclusions

Using a two-step solution combustion technique, it was possible to synthesize V_2O_5 rods with length to diameter ratio of 3–6. Pd nanoparticles of 20 nm size were deposited on the rods using wet-impregnation technique. Partial crystallization of V_2O_5 took place during the combustion step, whereas complete crystallization occurred during the calcination step. The changes in the crystallinity were investigated using TEM and XRD. The as-synthesized compound was found to contain a large amount of carbon deposits, as confirmed by EDX and TGA. The three materials namely the as-synthesized, the calcined compound and Pd-impregnated compounds were tested for three different environmental applications, i.e., oxidation of CO, adsorption, and photocatalytic degradation of dyes. The Pd-impregnated V_2O_5 showed high activity for CO oxidation and complete conversion occurred within 350°C. The as-synthesized V_2O_5 showed high rates of adsorption of cationic dyes and the adsorption was found to follow nth-order kinetics. Calcined-V_2O_5 was found to be photocatalytically active for the degradation of anionic and cationic dyes, and the rates of degradation were determined.

Acknowledgments

G. M. gratefully acknowledges Department of Science and Technology, Government of India, for the Swarnajayanti fellowship. P. A. D. thanks the Bristol-Myers Squibb for the graduate fellowship.

Literature Cited

1. Nova I, Ciardelli C, Tronconi E, Chatterjee D, Brandl-Konrad B. NH_3-SCR of NO over a V-based catalyst: low-T redox kinetics with NH_3 inhibition. *AIChE J*. 2006;52:3222–3233.
2. Andersson SL, Gabrielsson PTL, Odenbrand CUI. Reducing NO_x in diesel exhaust by SCR technique: experiments and simulations. *AIChE J*. 1994;40:1911–1919.
3. Fino D, Russo N, Badini C, Saracco G, Specchia V. Effect of active species mobility on soot-combustion over Cs-V catalysts. *AIChE J*. 2003;49:2173–2180.

4. Rao TVM, Deo G. Kinetic parameter analysis for propane ODH: V_2O_5/Al_2O_3 and MoO_3/Al_2O_3 catalysts. *AIChE J*. 2007;53:1583–1549.
5. Taufiq-Yap YH, Waugh KC. A study of the nature of oxidant in V_2O_5-MoO_3/Al_2O_3 catalyst. *Chem Eng Sci*. 2001;56:5787–5792.
6. Reddy BM, Khan A, Yamada Y, Kobayashi T. Raman and X-ray photoelectron study of CeO_2-ZrO_2 and V_2O_5/CeO_2-ZrO_2 catalysts. *Langmuir*. 2003;19:3025–3030.
7. Sohn JR, Doh IJ, Pae YI. Spectroscopic study of V_2O_5 supported on zirconia and modified with WO_3. *Langmuir*. 2008;18:6280–6288.
8. Reddy EP, Rojas TC, Fernandez A. Transmission electron microscopy and energy-dispersive X-ray spectroscopy study of V_2O_5/TiO_2-ZrO_2 catalysts. *Langmuir*. 2000;16:4217–4221.
9. Pieck CL, del Val S, Granados ML, Banares MA, Fierro JLG. Bulk and surface structures of V_2O_5/ZrO_2 systems and their revelance for *o*-xylene oxidation. *Langmuir*. 2002;18:2642–2648.
10. Phil HH, Reddy MP, Kumar PA, Ju LK, Hyo JS. SO_2 resistant antimony promoted V_2O_5/TiO_2 catalyst for NH_3-SCR of NO_x at low temperatures. *Appl Catal B*. 2007;78:301–308.
11. Gotic M, Popovic S, Ivanda M, Music S. Sol-gel synthesis and characterization of V_2O_5 powders. *Mater Lett*. 2003;57:3186–3192.
12. Fei H, Zhou H, Wang J, Sun P, Ding D, Chen T. Synthesis of hollow V_2O_5 microspheres and applications to photocatalysis. *Solid State Sci*. 2008;10:1276–1284.
13. Zhau Y, Qiu Z, Lu M, Zhang A, Ma Q. Preparation and characterization of V_2O_5 macro-plates. *Mater Lett*. 2007;61:4073–4405.
14. Zou CW, Yan XD, Patterson DA, Emanuelsson EAC, Bian JM, Gao W. Temperature sensitive crystallization of V_2O_5: from amorphous film to β-V_2O_5 nanorods. *CrystEngComm*. 2010;12:691–693.
15. Diaz-Guerra C, Piqueras J. Termal deposition growth and luminescence properties of single-crystalline V_2O_5 elongated nanostructures. *Cryst Growth Des*. 2008;8:1031–1034.
16. Avansi W Jr, Ribeiro C, Leite ER, Mastelaro VR. Vanadium pentaoxide nanostructures: an effective control of morphology and crystal structure in hydrothermal conditions. *Cryst Growth Des*. 2009;9: 3626–3631.
17. Su Q, Huang CK, Wang Y, Fan YC, Lu BA, Lan W, Wang YY, Liu XQ. Formation of vanadium oxides with various morphological features by chemical vapour deposition. *J Alloys Compd*. 2009;475: 518–523.
18. Si R, Stephanopoulos M. Shape and crystal-plane effects of nanoscale ceria on the catalytic activity of Au-CeO_2 catalysts for the water-gas shift reaction. *Angew Chem Int Ed Engl*. 2008;47:2884–2887.
19. Kunming J, Huili Z, Wencui L. Effect of the morphology of the ceria support on the activity of Au/CeO_2 catalysts for CO oxidation. *J Catal*. 2008;29:1089–1092.
20. Hargreaves JSJ, Hutchings GJ, Joyner RW, Kiely CJ. The relationship between catalyst morphology and performance in the oxidative coupling of methane. *J Catal*. 1992;135:576–595.
21. Roy S, Baiker A. NO_x storage-reductions catalysis: from mechanism and materials to material properties to storage-reduction performance. *Chem Rev*. 2009;109:4054–4091.
22. Calatayud M, Mguig B, Minot C. Modeling catalytic reduction of NO by ammonia over V_2O_5. *Surf Sci Rep*. 2004;55: 169–236.
23. Gorte RJ. Ceria in catalysis: from automotive applications to the water-gas shift reaction. *AIChE J*. 2010;56:1126–1135.
24. Muncrief RL, Kabin KS, Harold MP. NO_x storage and reduction with propylene on Pt/BaO/Al_2O_3. *AIChE J*. 2004;50:2526–2540.
25. Clayton RD, Harold MP, Balakotaiah V. Performance features of Pt/BaO lean NOx trap with hydrogen as reductant. *AIChE J*. 2009;55: 687–700.
26. Abdul-Kareem HK, Silveston PL, Hudgins RR. Forced recycling of the catalytic oxidation of CO over a V_2O_5 catalyst. Part I. Concentration cycling. *Chem Eng Sci*. 1980;35:2077–2084.
27. Abdul-Kareem HK, Silveston PL, Hudgins RR. Forced recycling of the catalytic oxidation of CO over a V_2O_5 catalyst. Part II. Temperature cycling. *Chem Eng Sci*. 1980;35:2085–2088.
28. Wu Z, Dong F, Lui Y, Wang H. Enhancement of the visible light photocatalytic performance of C-doped TiO_2 by loading with V_2O_5. *Catal Commun*. 2009;11:82–86.
29. Liu J, Wang R, Li S. Preparation and characterization of the TiO_2-V_2O_5 photocatalyst with visible light activity. *Rare Met*. 2006;25: 636–642.
30. Hu R, Zhong S. Photocatalytic reaction for synthesizing methacrolein from C_3H_8 and CO_2 on Cu/V_2O_5-TiO_2/SiO_2. *J Fuel Chem Technol*. 2005;33:376–341.
31. Karunakaran C, Senthilvelan S. Vanadia-catalyzed solar photooxidation of aniline. *J Colloid Interface Sci*. 2005;289:466–471.
32. Silversmit G, Depla D, Poelman H, Marin GB, Gryse RD. Determination of the V2p XPD binding energies for different vanadium oxidation states (V^{5+} to V^0). *J Electron Spectrosc*. 2004;135:167–175.
33. Zeggane S, Delamar M. XPS study of the penetration and reaction speed of polymer derivatization reagents. *Appl Surf Sci*. 1988;31: 151–156.
34. Ballutaud D, Simon N, Girard H, Rzepka E, Fabre B. Photoelectron spectroscopy of hydrogen at the polycrystalline diamond surface. *Diamond Relat Mater*. 2006;15:716–719.
35. Deshpande PA, Hegde MS, Madras G. Pt and Pd ions as highly active sites for the water-gas shift reaction over combustion synthesized zirconia and zirconia-modifed ceria. *Appl Catal B*. 2010;96: 83–93.
36. Pierre D, Dang W, Flytzani-Stephanopoulos M. The importance of strongly bound Pt-CeO_x species for the water-gas shift reaction: catalyst activity and stability evolution. *Top Catal*. 2007;46:363–373.
37. Zhau F, Zhao X, Liu Y, Yuan C, Li L. Synthesis of millimeter range orthorhombic V_2O_5 nanowires and impact of thermodynamic and kinetic properties of the oxidants on the synthetic process. *Eur J Inorg Chem*. 2008;2506–2509.
38. Iwamoto M, Yoda Y, Yamazoe N, Seiyama T. Study of metal oxide catalysts by temperature programmed desorption, Part 4. Oxygen desorption on various metal oxides. *J Phys Chem*. 1978;82:2564–2570.
39. Mori K, Miyamoto A, Murakami Y. Catalytic reactions on well-characterized vanadium oxide catalysts, Part 4. Oxidation of butane. *J Phys Chem*. 1985;89:4265–4269.
40. Taufiq-Yap YH, Waugh KC. Temperature programmed techniques study on the nature of the oxidant in/on V_2O_5 catalyst. *React Kinet Catal Lett*. 2006;89:9–19.
41. Lewis KB, Oyama ST, Somorjai GA. TPD studies of vanadium oxide films deposited on gold. *Surf Sci*. 1991;52:241–248.
42. Hermann K, Witko M, Druzinic R. Electronic properties, structure and adsorption at vanadium oxide: density functional theory studies. *Faraday Discuss*. 1999;114:53–66.
43. Hermann K, Witko M, Druzinic R, Tokarz R. Oxygen vacancies at oxide surfaces: ab initio density functional theory studies on vanadium pentoxide. *Appl Phys A*. 2001;72:429–442.
44. Xiao Y, Liu Q, Liu Z, Huang Z, Gou Y, Yang J. Roles of lattice oxygen in V_2O_5 and activated coke in SO_2 removal over coke-supported V_2O_5 catalysts. *Appl Catal B*. 2008;82:114–119.
45. Shustorovich E, Sellers H. The UBI-QEP method: a practical theoretical approach to understanding chemistry on transition metal surfaces. *Surf Sci Rep*. 1998;31:1–119.
46. Yin X, Han H, Gunji I, Endou A, Ammal SSC, Kubo M, Miyamoto A. NH_3 adsorption on the Bronsted and Lewis acid sites of V_2O_5(010): a periodic density functional theory. *J Phys Chem B*. 1999;103:4701–4706.
47. Yong X, Zhen-yu L, Qing-ya L, Xin-yan X, Jiang-chen W. Distribution of V_2O_5 on activated cokes measured by chemical adsorption. *J Fuel Chem Technol*. 2008;36:257–260.
48. Leyva-Ramos R, Rivera-Utrilla J, Medellin-Castillo NA, Sanchez-Polo M. Kinetic modeling of fluoride adsorption from aqueous solution onto bone char. *Chem Eng J*. 2010;158: 458–467.
49. Karthikeyen T, Rajgopal S, Miranda RL. Chromium (VI) adsorption from aqueous solution by *Hevea Brasilinesis* sawdust activated carbon. *J Hazard Mater*. 2005;124:192–199.
50. Vinu R, Akki SU, Madras G. Investigation of dye functional group on the photocatalytic degradation of dyes by nano-TiO_2. *J Hazard Mater*. 2010;176:765–773.

Manuscript received July 16, 2010, and revision received Aug. 18, 2010.